Optimal Shape Design of Microwave Device Using FDTD and Design Sensitivity Analysis

Young-Seek Chung, Changyul Cheon, *Member, IEEE*, Il-han Park, and Song-yop Hahn, *Senior Member, IEEE*

***Abstract*—In this paper, a novel optimal shape design method is proposed using the finite-difference time-domain (FDTD) method and the design sensitivity analysis to obtain broad-band characteristics of microwave devices. In shape design problem, the nodes that describe the shape of geometry to be optimized are taken as design variables. The design sensitivity is evaluated using the adjoint variable equation that is obtained from a terminal-value problem. The adjoint equation can be solved by the FDTD technique with the backward time scheme. With this method, a Ka-band unilateral fin line is tested to show validity.**

***Index Terms*—Design sensitivity analysis, FDTD, optimal shape design algorithm.**

I. Introduction

SINCE the 1970's, the concept of design sensitivity analysis (DSA) has been studied and presented in structural engineering [1]. The DSA concerns the relationship between the objective function and design variables, in which the objective function is represented in a form of the derivatives of design variables. In the shape optimization problem, the objective function can be a performance or a response of the device and the design variable is the shape of the device. There are two procedures, i.e., the direct differentiation and adjoint variable methods, to evaluate the design sensitivity. First, the direct differentiation method is used to obtain the design sensitivity from a direct differentiation of the system equation with respect to design variables. The disadvantage of this method is that it requires solving the system equation for each design variable. Second, the adjoint variable method is used to introduce the adjoint variable vector and derive the adjoint variable equation. Once this adjoint variable equation is solved, design sensitivities can be calculated, which requires only a moderate amount of computation.

Recently, optimization methods for waveguide structures based on vector finite-element method (FEM) and the DSA in the frequency domain was proposed by Lee *et al.* [2]–[4]. The methods may be appropriate to obtain optimal shape of device that gives proper performances in a narrow frequency range, not in a wide frequency range. In this paper, in order to design the optimal shape working in a wide frequency range, we propose a new shape design algorithm based on the finite-difference time-domain (FDTD) technique that is one of the popular time-domain analysis techniques [5].

When we use the FDTD technique in the optimizing process, however, the design sensitivity cannot be obtained directly because the adjoint variable equation in the FDTD algorithm cannot be derived in a straightforward manner, while that in FEM can be. Therefore, we employ an adjoint variable equation that is derived from system matrices of finite-element time-domain (FETD) formulation. This adjoint variable equation is then transformed as the coupled Maxwellian curl equations. These curl equations are solved by the FDTD method and the backward time scheme.

In an optimal shape design problem, since the shapes are allowed to change at each design iteration, the structured grids are not adequate to model the complex shapes. In this paper, the unstructured quadrilateral meshes are used to model the complex shape of problems. In order to deal with the general shape problems, the discrete surface integral (DSI) method or planar generalized Yee (PGY) algorithm [6], [7] has been employed in the unstructured design space and the standard Yee algorithm in the rest of space.

To demonstrate the validity of the method, we applied the shape optimization method to a Ka-band unilateral fin-line structure to obtain broad-band transition between the rectangular waveguide and the fin line with a quarter-wave transformer. The objective function was defined as the transmitted energy at the fin gap, which should be maximized, and in order to reduce the computing time, the transparent field source scheme [8] was introduced.

To reduce the computational domain, the Berenger's perfectly matched layer (PML) technique [9] was adopted when the electromagnetic fields and adjoint variables are analyzed.

II. DSA Based on the FETD

From Maxwell's equations, the vector wave equation is written as

$$\nabla \times \frac{1}{\mu_r} \nabla \times \vec{E} + \frac{\varepsilon_r}{c_0^2} \frac{\partial^2}{\partial t^2} \vec{E} = -\mu_0 \frac{\partial}{\partial t} \vec{J} \tag{1}$$

where μ_r denotes relative permeability, ε_r denotes relative permittivity, c_0 denotes velocity of light, and $\vec{J}$ denotes an impressed electric current density. Using the edge elements and Galerkin's formula, one can discretize the vector wave equation and construct the system equation with initial conditions as

$$[M]\{\ddot{e}\} + [K]\{e\} = \{Q\} \tag{2a}$$

$$e(0) = 0$$

$$\dot{e}(0) = 0 \tag{2b}$$

Manuscript received March 6, 2000; revised August 21, 2000. This work was supported in part by the Korean Ministry of Science and Technology under the Creative Research Initiative Program, Seoul, Korea.

Y.-S. Chung and S. Hahn are with the School of Electrical Engineering, Seoul National University, Seoul 151-742, Korea.

C. Cheon is with the Department of Electronics, University of Seoul, Seoul 130-743, Korea.

I. Park is with the School of Electrical and Computer Engineering, Sungkyunkwan University, Kyunggi-do 440-746, Korea.

Publisher Item Identifier S 0018-9480(00)10722-7.

where $\dot{}$ denotes the time derivative and e the tangential electric field along the edge. The elemental matrices and load vector of (1) contain the integral of the following:

$$M_{ij}^e = \frac{1}{c_0^2}\int_{\Omega^e} \varepsilon_r \vec{N}_i \cdot \vec{N}_j \, d\Omega \tag{3a}$$

$$K_{ij}^e = \int_{\Omega^e} \frac{1}{\mu_r}(\nabla \times \vec{N}_i)\cdot(\nabla \times \vec{N}_j)\, d\Omega \tag{3b}$$

$$Q_i^e = -\mu_0 \int_{\Omega^e} \vec{J}\cdot \vec{N}_i \, d\Omega \tag{3c}$$

where $\vec{N}_i$ is a vector basis function that has a tangential component only along the ith edge.

In order to obtain a desired response and estimate the design process, an objective function F is defined as

$$F(e, p) = \int_{\Omega_m} \left(\int_0^T G(e, p)\, dt \right) d\Omega \tag{4}$$

where T is a fixed final time and G an arbitrary differentiable function of e and p. In an optimal shape design problem, the design variable p is defined as the position vector of the node of the shape that is to be optimized. Ω_m is a observation domain where the objective function is evaluated. The DSA can be considered as an evaluation of the partial derivative values of the objective function with respect to the design variables. The first variation of F is written as

$$\begin{aligned}\delta F &= \frac{\partial F}{\partial \{e\}^T}\{\delta e\} + \frac{\partial F}{\partial \{p\}^T}\{\delta p\} \\ &= \int_0^T \left[\frac{\partial G}{\partial \{e\}^T}\{\delta e\} + \frac{\partial G}{\partial \{p\}^T}\{\delta p\} \right] dt \end{aligned} \tag{5}$$

and the sensitivity is represented as

$$\frac{\partial F}{\partial p_i} = \int_0^T \left[\frac{\partial G}{\partial e}\frac{\partial e}{\partial p_i} + \frac{\partial G}{\partial p_i} \right] dt, \qquad i = 1, 2, \ldots, n_p \tag{6}$$

where n_p is the number of p. In general, the field variable e has an implicit relation with the design variables and $\partial e/\partial p_i$ can be obtained using an indirect method. There are two methods to calculate (6), which are the direct differentiation method and the adjoint variable method. In this paper, the adjoint variable method [10] is favorable due to its computational efficiency.

Premultiplying (2a) by the transpose of an adjoint variable vector $\lambda = \lambda(t)$ and integrating over the time interval $[0, T]$, we obtain

$$\int_0^T \lambda^T \Big[[M(p)]\{\ddot{e}\} + [K(p)]\{e\} - \{Q(p)\} \Big] dt = 0. \tag{7}$$

Since this equation must hold for arbitrary λ, which is independent of design variable p, take the first variation of (7) to obtain the relationship and rewrite, using the integration by parts

$$\begin{aligned}&\left(\lambda^T[M]\left\{\frac{\partial \dot{e}}{\partial p}\right\} - \dot{\lambda}^T[M]\left\{\frac{\partial e}{\partial p}\right\} \right)\Bigg|_{t=T} + \int_0^T \\ &\quad \cdot \left(\ddot{\lambda}^T[M] + \lambda^T[K] \right)\left\{\frac{\partial e}{\partial p}\right\} dt = \int_0^T \lambda^T \left[\frac{\partial R}{\partial p}\right] dt \end{aligned} \tag{8}$$

where λ^T is the transpose of λ. Since (8) must hold for arbitrary $\lambda(t)$, λ may be chosen so that using the optimal control theory [11], [12], the coefficients of terms involving $(\partial e/\partial p)|_{t=T}$, $(\partial \dot{e}/\partial p)|_{t=T}$ and $(\partial e(t)/\partial p)$ in (6) and (8), are equal. To find such a $\lambda(t)$ requires that

$$[M]\{\ddot{\lambda}\} + [K]\{\lambda\} = \left\{\frac{\partial G}{\partial e}\right\}^T \tag{9a}$$

$$\lambda(T) = 0$$

$$\dot{\lambda}(T) = 0 \tag{9b}$$

where $0 \le t < T$. Equation (9a) is an adjoint equation of (2a) and (9b) is a terminal condition on λ for solving (9a). Thus, the above equation is a terminal-value problem. The adjoint equation (9a) has a same discretized form as (2a), except the forcing term and terminal condition. The same boundary conditions in (2b) must be applied to (8), except the absorbing boundary condition (ABC). To deal with terminal conditions, the backward time scheme $\tau \equiv T - t$ is introduced. With this variable, $d/dt \equiv -d/d\tau$, $d^2/dt^2 \equiv d^2/d\tau^2$, and the terminal conditions of (9b) for the t variable become initial conditions in τ. Thus, the backward time initial boundary-value problem for the $\overline{\lambda}(\tau) = \lambda(T - t)$ is

$$[M]\left\{\ddot{\overline{\lambda}}\right\} + [K]\{\overline{\lambda}\} = \left\{\frac{\partial G}{\partial e}(T - \tau)\right\}^T \tag{10a}$$

$$\overline{\lambda}(0) = 0$$

$$\dot{\overline{\lambda}}(0) = 0 \tag{10b}$$

where the superscript $^-$ denotes a backward time variable and $0 < \tau < T$. Thus, the adjoint equation is physically the same as the original equation, but with a backward time step and a load vector. Using (6), (8), and $\overline{\lambda}(\tau)$, we obtain the design sensitivity as

$$\frac{dF}{dp} = \int_{\Omega_m}\int_0^T \left(\lambda^T(t)\frac{\partial R(p, t)}{\partial p} + \frac{\partial G(e, p, t)}{\partial p} \right) dt\, d\Omega \tag{11}$$

where

$$R(p, t) = \{Q(t)\} - [M(p)]\{\ddot{\tilde{e}}\} - [K(p)]\{\tilde{e}\}. \tag{12}$$

The elemental matrices (3a)–(3c) are dependent on the geometry of the problem. That is, they can be explicitly represented as functions of geometry and material properties of the model. Therefore, we can calculate a derivative of (3a)–(3c) with respect to p and obtain the sensitivity information.

III. DSA Based on the FDTD

In above, the design sensitivity, which is a derivative of the objective function with respect to the design variables, was able to be derived using the FETD and the adjoint variable method. In this section, we derive the design sensitivity using the FDTD technique from the uniqueness theorem. The electric and magnetic fields can be calculated by applying the FDTD technique to the Maxwell's equations. Note that from the uniqueness theorem, the solutions that are obtained using the FDTD must theoretically be equal to the ones from the FETD. Therefore, the discretized matrices of (2a) can be considered as the corresponding

operators to the FDTD scheme. Therefore, we can change (9a) as the coupled Maxwellian curl equations as follows:

$$\nabla \times \vec{\lambda}^E = -\frac{\partial \vec{\lambda}^B}{\partial t} \tag{13a}$$

$$\nabla \times \vec{\lambda}^H = \frac{\partial \vec{\lambda}^D}{\partial t} + \vec{J}^{\lambda} \tag{13b}$$

subject to

$$\vec{\lambda}^E(T) = 0 \quad \vec{\lambda}^E(T) = 0 \tag{13c}$$

where $\vec{\lambda}^E$ and $\vec{\lambda}^H$ are adjoint electric- and magnetic-field intensity vector, and these adjoint variable vectors satisfy the constitutive relation the same as the electromagnetic-field vectors. That is, $\vec{\lambda}^D = \varepsilon \vec{\lambda}^E$ and $\vec{\lambda}^B = \mu \vec{\lambda}^H$. In (13b), $\vec{J}^{\lambda}$ is a pseudoelectric current density vector and can be obtained using the relation of

$$\left.\frac{\partial G}{\partial e}\right|_{\Omega_m} = -\mu_0 \int_{\Omega_m} \vec{N}_i \cdot \vec{j}^{\lambda}\, d\Omega. \tag{14}$$

Since G is a function of e, p, and t, the left-hand side of (14) is known. Since the observation point is located at the edge of an element, a pseudoelectric current density can be defined as

$$\left.\vec{J}^{\lambda}\right|_{\Omega_m} = \vec{J}^{\lambda} \delta(x - x_m, y - y_m, z - z_m) \tag{15}$$

where (x_m, y_m, z_m) is the center of the mth edge, which is defined as observation plane and $\delta(x, y, z)$ is a delta function. Then, if the only y-directional fields are observed, the relation on the left-hand side of (14) becomes

$$-\mu_0 \int_{\Omega_m} \vec{N}_i \cdot \vec{j}^{\lambda}\, d\Omega = -\mu_0 j_y^{\lambda} \tag{16}$$

and using (14) and (16), a pseudoelectric current density is obtained from

$$J_y^{\lambda}(t) = -\frac{1}{\mu_0} \int_0^t \frac{\partial G(t')}{\partial e}\, dt'. \tag{17}$$

Note that $J_y^{\lambda}(t)$ is an infinitesimal pseudoelectric current element. Thus, this pseudocurrent density is not an exact source of the FDTD scheme. In order to apply $J_y^{\lambda}(t)$ to the FDTD solver, the FDTD pseudocurrent density can be represented as follows [13]:

$$\left. J_{y,\,\mathrm{FDTD}}^{\lambda} \right|_{i,j}^{n} = \frac{J_y^{\lambda}(n\Delta t)}{\Delta x \Delta y \Delta z}. \tag{18}$$

Using the backward time scheme, (13a)–(13c) can be rewritten as

$$\nabla \times \vec{\overline{\lambda}}^E = \frac{\partial \vec{\overline{\lambda}}^B}{\partial \tau} \tag{19a}$$

$$\nabla \times \vec{\overline{\lambda}}^H = -\frac{\partial \vec{\overline{\lambda}}^D}{\partial \tau} + \vec{\overline{J}}^{\lambda}{}_{\mathrm{FDTD}}(T - \tau) \tag{19b}$$

subject to

$$\vec{\overline{\lambda}}^E(0) = 0 \quad \vec{\overline{\lambda}}^H(0) = 0 \tag{19c}$$

where $\vec{\overline{J}}^{\lambda}{}_{\mathrm{FDTD}}(T - \tau)$ is time reversed of (17) and $0 < \tau < T$. Equations (19a) and (19b) have opposite signs from the original Maxwell's equations. These Maxwellian curl equations can be discretized using the central-difference relation in time and space as follows for the TE case:

$$\begin{aligned} \overline{\lambda}_z{}^H\big|_{i,j}^{n+1/2} = {} & \overline{\lambda}_z{}^H\big|_{i,j}^{n-1/2} + \frac{\Delta\tau}{\mu_0} \\ & \cdot \left(\frac{\overline{\lambda}_y{}^E\big|_{i+1/2,j}^{n} - \overline{\lambda}_y{}^E\big|_{i-1/2,j}^{n}}{\Delta x} \right. \\ & \left. - \frac{\overline{\lambda}_x{}^E\big|_{i,j+1/2}^{n} - \overline{\lambda}_x{}^E\big|_{i,j-1/2}^{n}}{\Delta y} \right) \end{aligned} \tag{20a}$$

$$\begin{aligned} \overline{\lambda}_x{}^E\big|_{i,j}^{n+1} = {} & \overline{\lambda}_x{}^E\big|_{i,j}^{n} - \frac{\Delta\tau}{\varepsilon} \left(\frac{\overline{\lambda}_x{}^E\big|_{i,j+1/2}^{n+1/2} - \overline{\lambda}_z{}^H\big|_{i,j-1/2}^{n+1/2}}{\Delta y} \right) \\ & + \frac{\Delta\tau}{\mu_0 \varepsilon}\, \overline{J}_{x,\,\mathrm{FDTD}}^{\lambda}\big|_{i,j}^{T-n-1/2} \end{aligned} \tag{20b}$$

$$\begin{aligned} \overline{\lambda}_y{}^E\big|_{i,j}^{n+1} = {} & \overline{\lambda}_y{}^E\big|_{i,j}^{n} + \frac{\Delta\tau}{\varepsilon} \left(\frac{\overline{\lambda}_x{}^E\big|_{i+1/2,j}^{n+1/2} - \overline{\lambda}_x{}^E\big|_{i-1/2,j}^{n+1/2}}{\Delta x} \right) \\ & + \frac{\Delta\tau}{\mu_0 \varepsilon}\, \overline{J}_{y,\,\mathrm{FDTD}}^{\lambda}\big|_{i,j}^{T-n-1/2}. \end{aligned} \tag{20c}$$

Since the FDTD pseudocurrent source is a known function, $\overline{\lambda}_z{}^H(\tau)$, $\overline{\lambda}_x{}^E(\tau)$ and $\overline{\lambda}_y{}^E(\tau)$ can be obtained. Note that τ is a backward time clock and, thus, the adjoint variables are time reversed. Therefore, the real-time adjoint variables are

$$\lambda_z^H(t) = \overline{\lambda}_z{}^H(T - t) \tag{21a}$$

$$\lambda_x^E(t) = \overline{\lambda}_x{}^E(T - t) \tag{21b}$$

$$\lambda_y^E(t) = \overline{\lambda}_y{}^E(T - t). \tag{21c}$$

In (21b) and (21c), $\lambda_x^E(t)$ and $\lambda_y^E(t)$ are defined at the center of edge and can be considered to be the same as the solutions $\lambda(t)$ of (9a). Inserting the field and adjoint variables into (11), the sensitivity information can be calculated in the same way as the FETD.

IV. Optimization Algorithm

Using the sensitivity information (11), we can perform the optimal shape design of a given geometry. However, since the objective function is dependent on the design variables in an implicit manner and the system equation is a nonlinear function of design variables, an iterative method is preferred to find the optimum value of the objective function. Among many optimization schemes, the steepest descent method is employed in this paper due to its simplicity. This method searches the optimal point, iteratively changing the design variables. The iterative updating process of the design variable is as follows:

$$p_i^{k+1} = p_i^k + \Delta p_i \tag{22}$$

where p_i^k denotes the design variable at the kth optimization iteration step, and Δp_i is the change of the design variable, which is defined as

$$\Delta p_i = l\hat{n} \tag{23}$$

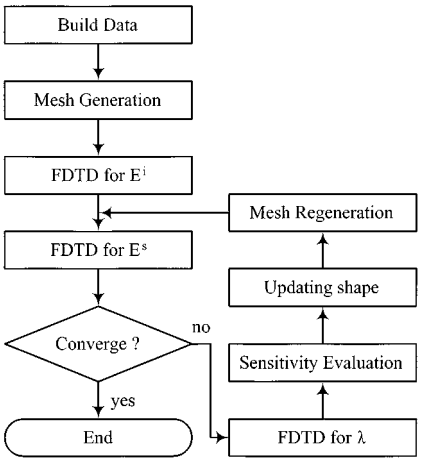

Fig. 1. Shape optimization algorithm using the FDTD technique. When regeneration meshes, the quality of grids should be maintained as uniformly as possible.

where $\hat{n}$ means the normalized directional vector and l denotes the length. Using (11) and (23)

$$\hat{n} = \frac{-dF/dp_i}{||dF/d[p]||} \tag{24}$$

$$l = \frac{F}{||dF/d[p]||} \tag{25}$$

where $||dF/d[p]||$ is the norm of the design variable vector. Using (23)–(25), (22) is rewritten as

$$p_i^{k+1} = p_i^k - \frac{F}{||dF/d[p]||^2}\frac{dF}{d[p]}. \tag{26}$$

From the updated design variable vector, we can obtain the new shape of the geometry to be optimized. Note that, in case of maximization of the objective function, the sign of (24) is not negative (i.e., $-$), but positive (i.e., $+$). This process is iteratively performed when the objective function value is satisfied with a given tolerance or converges. Fig. 1 shows the shape optimization algorithm using the FDTD technique and design sensitivity. At each optimization process, as the shape is changed, the grids should be regenerated.

V. DSI and Adjoint Variable Equations

In the optimal shape design process, the shape of geometry is changed and may be more complex. Thus, the rectangular or structured grids are not adequate and the unstructured ones are needed. However, using the unstructured grids, the standard Yee algorithm cannot be used. A general method to deal with the unstructured grids was introduced by Madsen [14]. This method is based on the integral forms of Maxwell's equations and the dual-grid concept, and the key idea is the projection scheme, which projects the face normal components into the dual edge. The electric fields are defined along each edge of primary grids, and magnetic fields are located along each edge of secondary grids. Similar to the electromagnetic fields, the DSI scheme has to be applied to the adjoint variables in the unstructured grid region. Rewriting (24a) and (24b) as integral forms

$$\frac{\partial}{\partial \tau}\int_{S_p} \vec{\lambda}^B \cdot d\vec{s}_p = \oint_{C_p} \vec{\lambda}^E \cdot d\vec{l}_p \tag{27a}$$

$$\frac{\partial}{\partial \tau}\int_{S_s} \vec{\lambda}^D \cdot d\vec{s}_s = -\oint_{C_s} \vec{\lambda}^H \cdot d\vec{l}_s + \int_{S_s} \vec{J}^{\lambda} \cdot d\vec{s}_s \tag{27b}$$

where S_p and S_s are the primary and secondary surfaces, respectively, and C_p and C_s are the primary and secondary contour over each face. The backward time derivative is approximated using a central-difference scheme and then (27a) and (27b) are discretized as follows:

$$\vec{\lambda}^B\Big|_i^{n+1/2} \cdot \hat{n}_p = \vec{\lambda}^B\Big|_i^{n-1/2} \cdot \hat{n}_p + \frac{\Delta\tau}{A_i^p}\sum_{k=1}^{N_i^p} \vec{l}_k^p \cdot \vec{\lambda}^E\Big|_{i,k}^n \tag{28a}$$

$$\vec{\lambda}^D\Big|_i^{n+1} \cdot \hat{n}_s = \vec{\lambda}^B\Big|_i^{n} \cdot \hat{n}_s - \frac{\Delta\tau}{A_i^s}\sum_{k=1}^{N_i^s} \vec{l}_k^s \cdot \vec{\lambda}^H\Big|_{i,k}^{n+1/2} + \vec{J}^{\lambda}\Big|_i^{n+1/2} \cdot \hat{n} \tag{28b}$$

where $\hat{n}_p$ and $\hat{n}_s$ are the normal vector to the primary and secondary face, and A_p and A_s are the area, and l_p and l_s are the edge vector of the primary and secondary grids. Since the grid is unstructured, there is a possibility that the edge vector is not parallel to the normal vector. Therefore, it is necessary to project the normal vector onto the edge vector, which is an interpolation concept. Using the projection scheme, the adjoint magnetic flux density vector is

$$\vec{\lambda}^B = \frac{\sum_{j=1}^{N_c}\sum_{i=1}^{N_e} |w_{i,j}|\,\vec{\lambda}^B{}_{i,j}}{\sum_{j=1}^{N_c}\sum_{i=1}^{N_e} |w_{i,j}|} \tag{29}$$

where N_c is the number of shared grids and N_e is the number of edges. $\vec{\lambda}^B{}_{i,j}$ is a local value with the ith and the jth corner shared by the face. $|w_{i,j}|$ is a weighting factor and, in this paper, we use $|w_{i,j}| = 1$. Finally, the adjoint magnetic flux density, which is parallel to the secondary grid, is obtained as

$$\vec{\lambda}^B \cdot \hat{s} = \frac{\sum_{j=1}^{N_c}\sum_{i=1}^{N_e} \vec{\lambda}^B{}_{i,j} \cdot \hat{s}}{N_c N_e}. \tag{30}$$

The adjoint magnetic-field intensity $\vec{\lambda}^H$ is calculated using the constitutive relation. Similarly, the adjoint electric-field intensity is

$$\vec{\lambda}^D \cdot \hat{p} = \frac{\sum_{j=1}^{N_c}\sum_{i=1}^{N_e} \vec{\lambda}^D{}_{i,j} \cdot \hat{p}}{N_c N_e}. \tag{31}$$

However, if the above DSI scheme is not well posed, the late-time oscillation may occur and be conditionally stable. In

order to make it unconditionally stable, we use the symmetric projection scheme [7].

VI. Modified PML for Adjoint Variable Equations

To solve the adjoint equation, the PML equations have to be modified. Otherwise, the adjoint fields are divergent according to the progress of the time step. This is due to the backward time scheme. Substituting E_x, E_y, H_{zx} and H_{zy} for λ_x^E, λ_y^E, λ_{zx}^H and λ_{zy}^H in the TE case, and using the backward time scheme, the PML equations for the adjoint variables are

$$-\varepsilon_0\frac{\partial\overline{\lambda}_x^E}{\partial\tau}+\sigma_y\overline{\lambda}_x^E=\frac{\partial\overline{\lambda}_z^H}{\partial y} \tag{32a}$$

$$-\varepsilon_0\frac{\partial\overline{\lambda}_y^E}{\partial\tau}+\sigma_x\overline{\lambda}_y^E=-\frac{\partial\overline{\lambda}_z^H}{\partial x} \tag{32b}$$

$$-\mu_0\frac{\partial\overline{\lambda}_{zx}^H}{\partial\tau}+\sigma_x^*\overline{\lambda}_{zx}^H=-\frac{\partial\overline{\lambda}_y^E}{\partial x} \tag{32c}$$

$$-\mu_0\frac{\partial\overline{\lambda}_{zy}^H}{\partial\tau}+\sigma_y^*\overline{\lambda}_{zy}^H=\frac{\partial\overline{\lambda}_x^E}{\partial y} \tag{32d}$$

where $\overline{\lambda}_z{}^H=\overline{\lambda}_{zx}{}^H+\overline{\lambda}_{zy}^H$. Applying the exponential time stepping to (32a)–(32d), however, we can find that the exponents are positive, which means that the adjoint variables in the PML region are exponentially divergent according to time stepping. This phenomenon is not physical and one can easily prove that the same ABC can be applied to the adjoint variable equation with the backward time scheme [15]. Therefore, the lossy materials in the PML region of adjoint variable equation have to absorb the outgoing adjoint waves. Thus, to absorb and decay the adjoint variables, the electric conductivities and magnetic losses have to be negative. That is,

$$\sigma_x\Rightarrow-\overline{\sigma}_x\quad\sigma_y\Rightarrow-\overline{\sigma}_y \tag{33a}$$

$$\sigma_x^*\Rightarrow-\overline{\sigma}_x^*\quad\sigma_y^*\Rightarrow-\overline{\sigma}_y^* \tag{33b}$$

where $\overline{\sigma}_x$, $\overline{\sigma}_y$, $\overline{\sigma}_x^*$ and $\overline{\sigma}_y^*$ are positive real constants. Inserting (33a) and (33b) into (32a)–(32d), the modified PML equations for adjoint variables can be represented as follows:

$$\varepsilon_0\frac{\partial\overline{\lambda}_x^E}{\partial\tau}+\overline{\sigma}_y\overline{\lambda}_x^E=-\frac{\partial\overline{\lambda}_z^H}{\partial y} \tag{34a}$$

$$\varepsilon_0\frac{\partial\overline{\lambda}_y^E}{\partial\tau}+\overline{\sigma}_x\overline{\lambda}_y^E=\frac{\partial\overline{\lambda}_z^H}{\partial x} \tag{34b}$$

$$\mu_0\frac{\partial\overline{\lambda}_{zx}^H}{\partial\tau}+\overline{\sigma}_x^*\overline{\lambda}_{zx}^H=\frac{\partial\overline{\lambda}_y^E}{\partial x} \tag{34c}$$

$$\mu_0\frac{\partial\overline{\lambda}_{zy}^H}{\partial\tau}+\overline{\sigma}_y^*\overline{\lambda}_{zy}^H=-\frac{\partial\overline{\lambda}_x^E}{\partial y}. \tag{34d}$$

Actually, these modified PML equations are successful in absorbing the adjoint variables when solving the adjoint equations by the FDTD. In three-dimensional problems, the adjoint variable method can be extended in the same way as before.

VII. Numerical Examples

The proposed optimization method was applied to the Ka-band unilateral fin line to obtain the broad-band transition taper shape. Since it was first proposed by Meier [16], the fin lines have been taken attention at millimeter wavelengths due to its large bandwidth, easy fabrication, and absence of radiation loss. Fig. 2 shows a typical unilateral fin-line structure. In order to minimize a dielectric discontinuity, the continuous quarter-wave transformer is adopted as Fig. 2.

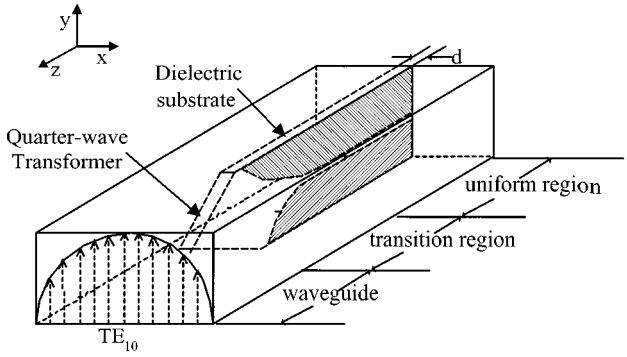

Fig. 2. Structure of a Ka-band unilateral waveguide to fin-line transition. In this paper, a continuous quarter-wave dielectric transformer was used for broad-band matching.

Since the fin line is located in the rectangular waveguide (WR28 in our example), it cannot support the TEM wave. Therefore, the impedance and propagation constant are dependent on frequency and the shape of the fin line. In order to reduce the reflection loss in a wide frequency range, the impedance has to be smoothly changed in the propagation direction, which results in a smooth taper shape. The impedance technique [17] is an approximate method to obtain the smooth transition based on the theory of small reflections.

When one solves the fin lines using the FDTD with an electric current source, the fields propagate for a long time. Thus, it takes many time iteration steps to require the fields below a tolerance. In this paper, we adopt the transparent field sources [8], which resemble the hard field sources without any scattering of energy. Although the time for solving impulse responses is required, the additional computational time is negligible compared with the total solving time. In our case, the Ricker wavelet is used for the driving transparent field source. The Ricker wavelet is defined as

$$p(t)=\left(1-2\left\{\pi f_R\left(t-T_R\right)\right\}^2\right)e^{-\left\{\pi f_R(t-T_R)\right\}^2} \tag{35}$$

where $f_R=34$ GHz and $T_R=1/f_R$. Fig. 3 shows the initial shape of the straightly tapered fin line and the design variable points. The observation plane was placed at the uniform fin gap. During the optimization process, the design variable points are allowed to move along the only y-direction holding the symmetric constraints. The objective function in this example is defined as

$$F=\int_{\Omega_m}\int_0^T\left(E_y^t(t)\right)^2\,dt\,dy \tag{36}$$

where $E_y^t(t)$ is the total transmitted electric field at the observation plane. If the transmitted energy is maximized, the return loss is minimized. Fig. 4 shows the values of the objective function normalized by the initial value as the iteration proceeds. The design process stopped at the 18th iteration due to the constraint of fin-line position, which is a limitation to maintain uniform grids, and Fig. 5 shows the change of fin-line shapes as the

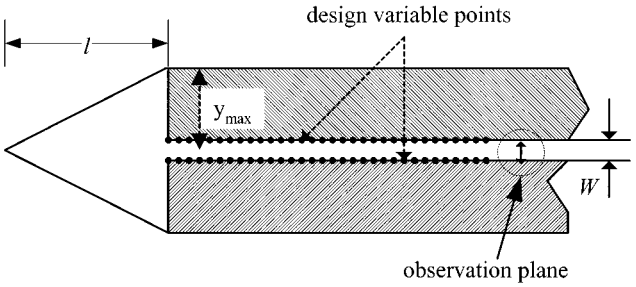

Fig. 3. Initial fin-line shape with straight taper. The design variable points are located on the edge of fin lines. The number of design variables is about 25. The y-axis movements of the upper design variable points are limited to the half-height of waveguide $y_{\max}$.

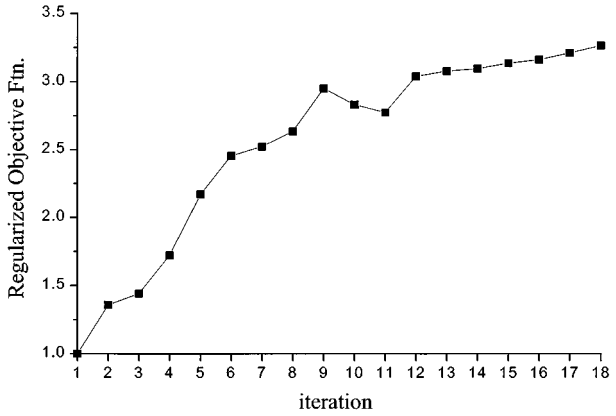

Fig. 4. Objective function value normalized by initial value versus the design iteration. Near the tenth iteration, the objective function is fluctuated. This is probably due to the quality of grids.

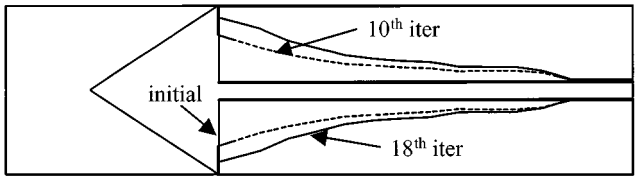

Fig. 5. Shape variation according to design iteration. The design process stopped at the eighteenth iteration to maintain the quality of grids as uniform as possible.

design iteration proceeds. The transition is flared toward the uniform waveguide section, as is expected. Fig. 6(a) and (b) shows the two-dimensional unstructured quadrilateral grids at the tenth and eighteenth design iteration steps, respectively. At the eighteenth grids, the number of elements is 697 and the number of edges is 1436, and the number of vertical layers is 21. Therefore, the number of unstructured brick elements is 14 637.

The number of total brick elements including the structured and PML grids is 51 429. Fig. 7 shows the magnitude of transmitted electric fields at the observation plane in the time domain. As is expected, the intensity of the transmitted field of the eighteenth step increases from that of the initial shape. Fig. 8 shows the results in the frequency domain, which are obtained by the Fourier transformation of Fig. 7. The transmitted energy of the eighteenth designed model is significantly increased compared

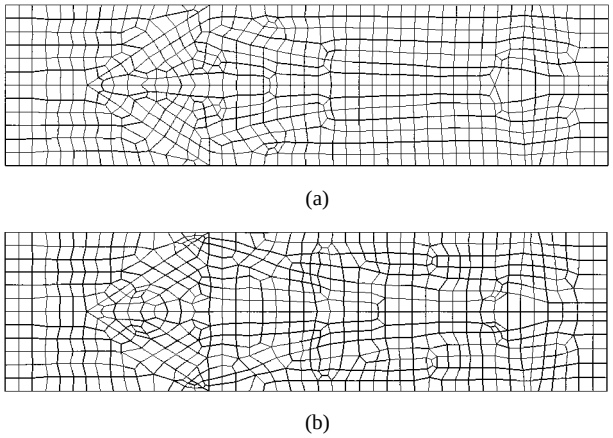

Fig. 6. Two-dimensional unstructured grids in the y–z-plane. The unstructured brick elements are generated by cascading in the vertical x-direction. (a) Tenth iteration. (b) Eighteenth iteration. As the last design variable point approaches the top or bottom of the waveguide, the small size grids are shown.

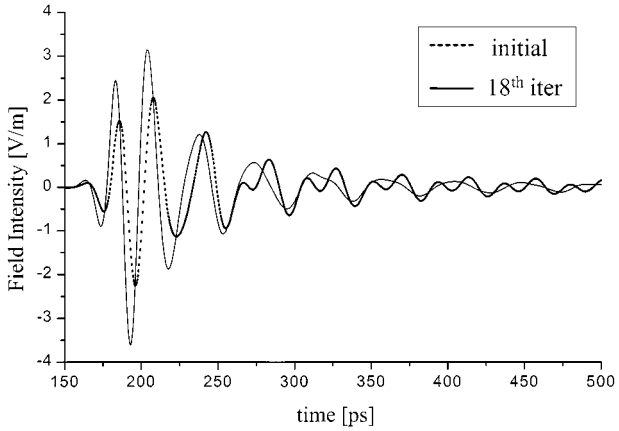

Fig. 7. Transmitted y-directional electric field in the time domain at the observation plane. The dotted line is in the case of the initial shape and the solid line is in the case of the eighteenth designed shape.

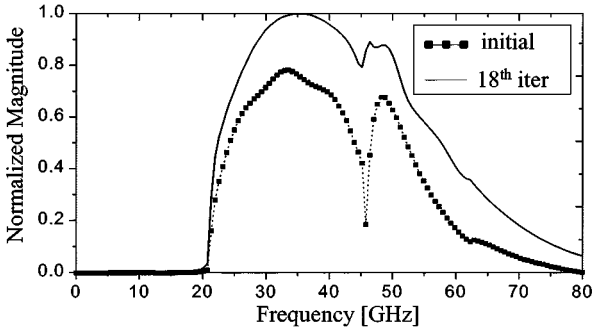

Fig. 8. Fourier transformation results of Fig. 7. The line with a square is in the case of the initial shape and the solid line is in the case of the eighteenth design.

to that of the initial model over a broad band, and any fields did not propagate below 21 GHz, which is the lowest cutoff frequency. Fig. 9 shows the analytically designed transition model using an exponential impedance taper. Fig. 10 shows the comparison of numerical simulations between the numerically designed and analytically designed models in the frequency domain.

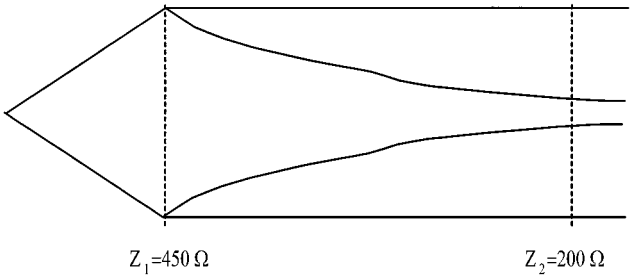

Fig. 9. Analytic fin-line shape with the exponential taper. The impedance function varies from 200 to 450 toward the waveguide section.

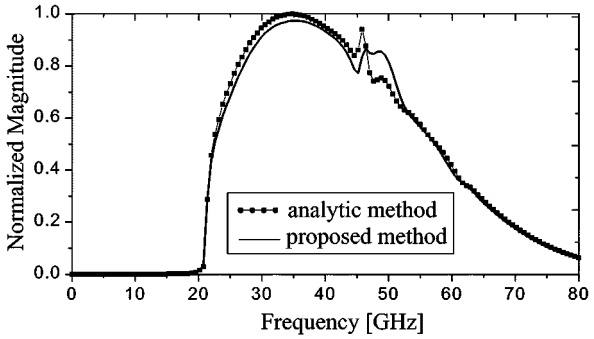

Fig. 10. Comparison of the Fourier transformation results between the proposed design method and analytic design.

TABLE I
CPU TIMES FOR ONE DESIGN PROCESS

Routine	time (sec)
Mesh Generation	4
Field Analysis	245
Adjoint Analysis	245
Sensitivity Analysis	40

The result of the analytic model gives slightly better performance than that of the numerically designed model. This is due to the moving limitations in the design variable points.

Table I represents the computational time that is measured on a 500-MHz Pentium III based on the Linux system. The CPU time of mesh generation is sufficiently negligible compared with that of field or adjoint analysis, and the CPU time of field analysis is equal to that of adjoint analysis.

VIII. CONCLUSIONS

A new optimal design method for the shape design of broad-band microwave devices based on the FDTD technique and DSA has been presented in this paper. Using the adjoint variable method, the design sensitivity was obtained by only two simulations at each design process, which is regardless of the number of design variables.

The proposed optimal shape design algorithm has been verified by designing a Ka-band unilateral fin-line transition. The final transition shape is similar to the exponential taper.

Lastly, it is obvious that the accurate evaluation of design sensitivity is prerequisite to optimal design process. In the numerical computation of design sensitivity, the reduction of discretization errors is very important. These errors are closely dependent on the quality of the unstructured grids. Therefore, in order to obtain more accurate design derivative and, thus, more optimized shape, the design region should be discretized as uniformly as possible.

REFERENCES

[1] E. J. Haug, K. K. Choi, and V. Komkov, *Design Sensitivity Analysis of Structural System*. New York: Academic, 1986.
[2] H.-B. Lee, "Computer aided optimal design methods for waveguide structures," Ph.D. dissertation, Seoul Nat. Univ., Seoul, Korea, 1995.
[3] Y. Lee, C. Cheon, and H. Kim, "Shape optimization of W/G structure for uniform field illumination," *IEEE Trans. Magn.*, vol. 34, pp. 3584–3587, May 1998.
[4] H. Lee, H. Jung, S. Hahn, C. Cheon, and K. Lee, "Shape optimization of H-plane waveguide tee junction using edge finite element method," *IEEE Trans. Magn.*, vol. 31, pp. 1928–1931, Mar. 1995.
[5] A. Taflove, *Computational Electrodynamics: The Finite-Difference Time-Domain Method*. Norwood, MA: Artech House, 1995.
[6] S. D. Gedney, "A comparison of the performance of finite difference time-domain, finite element time-domain, and discrete surface integral equation methods on high performance parallel computers," in *IEEE AP-S Int. Symp. Dig.*, vol. 1, 1994, pp. 384–387.
[7] S. D. Gedney, F. S. Lansing, and D. L. Rascoe, "Full wave analysis of microwave monolithic circuit devices using a generalized Yee-algorithm based on an unstructured grid," *IEEE Trans. Microwave Theory Tech.*, vol. 44, pp. 1393–1400, Aug. 1996.
[8] J. B. Schneider, C. L. Wagner, and O. M. Ramahi, "Implementation of transparent sources in FDTD simulations," *IEEE Trans. Antennas Propagat.*, vol. 46, pp. 1159–1168, Aug. 1998.
[9] J. P. Berenger, "A perfectly matched layer for the absorption of electromagnetic waves," *J. Comput. Phys.*, vol. 114, pp. 185–200, 1994.
[10] I.-H. Park, I.-G. Kwak, H.-B. Lee, S.-Y. Hahn, and K.-S. Lee, "Design sensitivity analysis for transient Eddy current problems using finite element discretization and adjoint variable method," *IEEE Trans. Magn.*, vol. 32, pp. 1242–1245, Mar. 1995.
[11] A. E. Bryson and Y. C. Ho, *Applied Optimal Control*. Bristol, PA: Hemisphere, 1975.
[12] A. C. Paul, A. Dutta, and C. V. Ramakrishnan, "Accurate computation of design sensitivities for dynamically loaded structures with displacement constraints," *AIAA J.*, vol. 34, no. 8, pp. 1670–1677, 1996.
[13] D. N. Buechler, D. H. Roper, C. H. Durney, and D. A. Christensen, "Modeling sources in the FDTD formulation and their use in quantifying source and boundary condition errors," *IEEE Trans. Microwave Theory Tech.*, vol. 43, pp. 810–814, Apr. 1995.
[14] N. Madsen, "Divergence preserving discrete surface integral methods for Maxwell's equations using nonorthogonal unstructured grids," *J. Comput. Phys.*, vol. 119, no. 1, pp. 34–45, 1995.
[15] Y. S. Chung, J. Ryu, C. Cheon, I. H. Park, and S. Y. Hahn, "Optimal design method for microwave device using time domain method and design sensitivity analysis: Part I. FETD case," in *Proc. IEEE CEFC*, 2000, p. 257.
[16] P. J. Meier, "Millimeter integrated circuits suspended in the E-plane of rectangular waveguide," *IEEE Trans. Microwave Theory Tech.*, vol. MTT-26, pp. 726–733, Oct. 1978.
[17] B. Bhat and S. K. Koul, *Analysis, Design and Applications of Fin Lines*. Norwood, MA: Artech House, 1987.
[18] C. A. W. Vale and P. Meyer, "Designing high-performance fin-line tapers with vector-based optimization," *IEEE Trans. Microwave Theory Tech.*, vol. 47, pp. 2467–2472, Dec. 1999.
[19] T. Itoh, G. Pelosi, and P. P. Silverster, *Finite Element Software for Microwave Engineering*. New York: Wiley, 1996.
[20] C. Sung-Hsien, R. Coccioli, Q. Yongxi, and T. Itoh, "A global finite-element time-domain analysis of active nonlinear microwave circuits," *IEEE Trans. Microwave Theory Tech.*, vol. 47, pp. 2410–2416, Dec. 1999.
[21] A. Nicolas, L. Nicolas, and C. Vollaire, "An explicit 2D finite element time domain scheme for electromagnetic wave propagation," *IEEE Trans. Magn.*, vol. 35, pp. 1538–1541, May 1999.
[22] K. S. Komisarek, N. N. Wang, A. K. Dominek, and R. Hann, "An investigation of new FETD/ABC methods of computation of scattering from three-dimensional material objects—An investigation of new FETD/ABC methods of computation of scattering from three-dimensional material objects," *IEEE Trans. Antennas Propagat.*, vol. 47, pp. 1579–1585, Oct. 1999.

[23] C.-T. Hwang and R.-B. Wu, "Treating late-time instability of hybrid finite-element/finite-difference time-domain method," *IEEE Trans. Antennas Propagat.*, vol. 47, pp. 227–232, Feb. 1999.
[24] K. Dongsoo, L. Hong-Bae, and T. Itoh, "A hybrid full-wave analysis of via hole grounds using finite difference and finite element time domain methods," in *IEEE MTT-S Int. Microwave Symp. Dig.*, vol. 1, 1997, pp. 89–92.
[25] U. Navsarlwala and S. D. Gedney, "An implicit finite element time-domain method with unconditional stability," in *IEEE AP-S Int. Symp. Dig.*, vol. 1, 1995, pp. 88–91.
[26] K. C. Gupta, R. Garg, I. Bahl, and P. Bhartia, *Microstrip Lines and Slotlines*. Norwood, MA: Artech House, 1996.
[27] J. Jin, *The Finite Element Method in Electromagnetics*. New York: Wiley, 1993.
[28] R. E. Collin, *Foundations for Microwave Engineering*. New York: McGraw-Hill, 1992.

Young-Seek Chung received the B.S., M.S. and Ph.D. degrees in electrical engineering from Seoul National University, Seoul, Korea, in 1989, 1991 and 2000, respectively.

From 1991 to 1996, he was with the Living System Laboratory, LG Electronics. From 1998 to 1999, he was a Teaching Assistant in electrical engineering at the Seoul National University. His current interests are the numerical analysis and design in the microwave and millimeter-wave devices.

Changyul Cheon (S'87–M'90) was born in Seoul, Korea, on April 5, 1960. He received the B.S. and M.S. degrees in electrical engineering from the Seoul National University, Seoul, Korea, in 1983 and 1985, respectively, and the Ph.D. degree in electrical engineering from The University of Michigan at Ann Arbor, in 1992. From 1992 to 1995, he was with the Department of Electrical Engineering, Kangwon National University, Chuncheon, Korea, as an Assistant Professor. He is currently an Associate Professor of electrical engineering at the University of Seoul. His group at the University of Soul is currently involved with the design and analysis of microwave and millimeter-wave passive device using FEM, FDTD and method of moments (MoM) techniques. He is also interested in high-power microwave systems for military and commercial applications.

Il-han Park received the B.S., M.S., and Ph.D. degrees in electrical engineering from Seoul National University, Seoul, Korea, in 1984, 1986 and 1990, respectively.

Since 1998, he has been with the School of Electrical and Computer Engineering, Sungkyunkwan University, Kyunggi-do, Korea. His main research interests are optimal design of electromagnetic devices and electromagnetic-field analysis.

Song-yop Hahn (S'79–M'79–SM'87) received the B.S. and M.S. degrees in electrical engineering from Seoul National University, Seoul, Korea, in 1963 and 1967, respectively, and the Ph.D. degree in electrical engineering from the Lorraine National Polytechnic Institute, Nancy, France, in 1979.

Since 1968, he has been with the School of Electrical Engineering, Seoul National University. His main research interests are optimal design of electromagnetic devices and development of superconducting electric machines.